J Electroceram (2015) 34:229–235
DOI 10.1007/s10832-014-9978-1

The origin of evolutionary device performance for GeGaInOx thin film transistor as a function of process pressure

Byung Du Ahn · Kwun-Bum Chung · Jin-Seong Park

Received: 21 August 2014 / Accepted: 29 October 2014 / Published online: 20 November 2014

Abstract This paper addresses changes in device performance for GeGaInOx (GGIO) thin film transistors deposited as a function of process pressures, and the mechanisms responsible for electronic band structure and defect states within sub-gap states. As the process pressure decreased from 5 to 1 mTorr during sputtering of the GGIO active layer, the saturation mobility increased from 6.51 to 11.18 cm^2/Vs and the sub-threshold swing value decreased from 0.64 to 0.21 V/decade. Conduction band areas measured by x-ray absorption spectroscopy in GGIO films increased as the total process pressure decreased from 5 to 1 mTorr, which can help charge transport in GGIO semiconductors. In addition, the ΔVth shift during positive bias temperature stability for 3 h was also enhanced from 17.5 to 6.2 V. This improvement can be attributed to the reduction of relative near conduction band edge defect states, which was found in not only at the GGIO films level by spectral ellipsometry, but also at the device level by the Meyer-Neldel rule.

Keywords Oxide semiconductor · Thin film transistor · Oxygen partial pressure · Stability

B. Du Ahn
School of Electrical and Electronic Engineering, Yonsei University, 50 Yonsei-ro, Seodaemun-gu, Seoul 120-749, South Korea

K.-B. Chung
Division of Physics and Semiconductor Science, Dongguk University, Seoul 100-715, South Korea

J.-S. Park (✉)
Division of Materials Science and Engineering, Hanyang University, 222, Wangsimni-ro Seongdong-gu, Seoul 133-719, South Korea
e-mail: jsparklime@hanyang.ac.kr

1 Introduction

Very recently, amorphous InGaZnO (a-IGZO) thin film transistors (TFTs), an alternative to amorphous Si and/or poly Si TFTs, have been selected as switching and driving TFTs for ultra-definition (UD, 4000×2000) liquid crystal display (LCD) panels and >55 in. active matrix organic light-emitting diode (AMOLED) panels by several mass production companies [1, 2]. However, as the oxide TFTs have been developed, many industries have required higher mobility and better device stability than a-IGZO TFTs for ultra-high resolution (UHD, 4000×8000) and fast-frame-rate (>240 Hz) applications. For achieving high-performance TFTs, numerous reports have been proposed including: development of novel oxide semiconductor materials using combinatorial material designs [3, 4], suggestion of new device structures with multiple active channels or double gates [5, 6], and introduction of new post treatment techniques [7]. Although it is well known that the physical and electrical properties of an oxide semiconductor itself can be initially determined during sputtering, recently most studies of oxide TFTs have focused on the new approach mentioned above.

Recently, two studies reported the effect of sputtering pressure on the electrical/physical properties in a-IGZO TFTs. Jeong et al. [8] reported that bulk defect can be reduced by decreasing the camber pressure. This improvement could be attributed to densification of the a-IGZO film, however information addressing how the densification of the a-IGZO film improved the electrical properties is lacking. Yasuno et al. [9] also reported that densification and roughness can be improved at a lower sputtering pressure, which also resulted in improvement saturation mobility (μ_{sat}) and sub-threshold swing (S.S.). However, there is still a lack of direct electronic structure evidence to support the variation electrical properties. It is well known that semiconductor properties strongly depend on the electronic structure, including defect states within sub-gap

states [10–12]. Kamiya et al. [11] reported that atomic and electronic structures were calculated for oxygen deficient in a-IGZO using density functional theory. Most oxygen deficiencies have low formation energies of 2–3.6 eV and form either deep, fully-occupied localized states near the valance band maximum or donor states. However, a small portion of oxygen deficiencies could form fully-occupied localized states even near the conduction band maximum (CBM). Therefore, it is vital to investigate sub-gap electronic structures to improve device performance, including stability. Many studies have suggested the charge trap issue in electronic structures, which causes bias-induced device instability [13–15]. Although the origin of charge traps is still unclear, oxygen-related defects have been strongly investigated as charge trap candidates, including: the charge trapping of photo-induced hole carriers, the creation of weak bond oxygen defects, and ionized oxygen vacancy defects [16–18]. However, there is still a lack of systematical investigations and direct experimental evidence to support any of these mechanisms.

In this work, germanium gallium indium oxides (GGIO), where the role of group-IV element Ge is the V_O suppressor or stabilizer to control the net electron concentration, were adopted to fabricate thin film transistors (TFTs). Bias temperature stress (BTS)-induced instability of GGIO TFTs was investigated as a function of process pressures. Spectral ellipsometry (SE), X-ray photoelectron spectroscopy (XPS), and X-ray adsorption spectroscopy (XAS) could suggest electronic structures, including defect states of GGIO films, depending on process pressures. In addition, the Meyer-Neldel rule could account for the relationship between state distribution density and BTS-induced instability at the device level.

2 Experiment

Amorphous GGIO TFTs have bottom gate and top contact configurations. Amorphous GGIO films as a channel layer were deposited on thermal SiO_2 (100 nm)/Silicon (heavily doped) substrates by radio frequency (RF) sputtering. The composition of the GGIO target was Ge:Ga:In=22:10:8 at.%. The RF power and relative oxygen flow rate ($[O_2]/[Ar+O_2]$) were 75 W and 0.05, respectively. The process pressure was varied from 1 to 5 mTorr. The GGIO layer thickness was about 50 nm, and patterned using a fine metal mask (FMM). Then, 100-nm-thick indium-tin-oxide (ITO, In/Sn=9:1 at.%) as source/drain (S/D) electrodes was sputtered onto the GGIO layer, which was patterned by FMM (with a channel width of 1000 μm and length of 150 μm). GGIO TFTs were then annealed at 300 °C for 1 h under an air.

The GGIO film compositions were investigated by Rutherford backscattering (RBS) analysis. High-resolution X-ray reflectivity (XRR) measurements were performed to double-check the roughness, density, and thickness of the GGIO thin films. In order to examine the electronic structure of GGIO film in the conduction band, X-ray absorption (XAS) was measured using coherent X-ray beams. XAS experiments were performed using total electron yield (TEY) mode, at the soft X-ray beamline available from the BL-11A Photon Factory in Japan. The SE measurements were performed by a rotating analyzer system with an auto retarder in the energy range of 0.75 eV to 6.4 eV with incident angles of 65°, 70°, and 75°. The chemical binding states in the core-level region were examined by X-ray photoelectron spectroscopy (XPS). The electrical characteristics were measured at room temperature in an air atmosphere using a HP4156C semiconductor parameter analyzer. To characterize the effects of positive bias temperature stress (PBTS) on the transfer characteristics of the GGIO TFTs, the devices were stressed with V_{GS} and V_{DS} set to 20 V and 0.1 V at 60 °C (substrate temperature), respectively. The maximum stress duration was 10,800 s.

3 Results and discussion

Figure 1 shows the representative transfer characteristics of GGIO TFTs deposited under different process pressures. Table 1 summarizes the principle TFT characteristics of the three devices. The field effect mobility (μ_{SAT}) and threshold voltage (V_{th}) in the linear region (V_{DS}=0.1 V) were calculated by fitting a straight line to the plot of the square root of I_{DS} versus V_{GS}, according to the expression for a field-effect transistor [19],

$$I_{DS} = \left(\frac{\mu_{FE} W C_i}{L}\right)\left[(V_{GS}-V_{th})V_{DS}-\frac{V_{DS}^2}{2}\right] \quad (1)$$

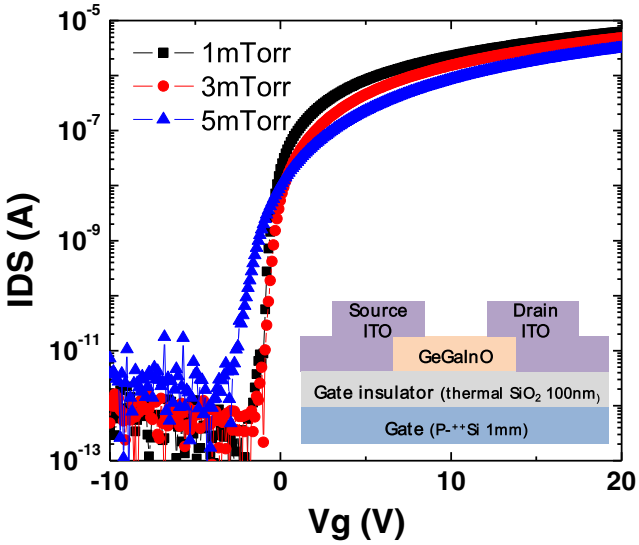

Fig. 1 Representative transfer characteristics of GGIO TFTs deposited at different process pressures (**a**) 1 mTorr, (**b**) 3 mTorr, and (**c**) 5 mTorr and schematic diagram of GIGO TFTs (inset)

Table 1 Comparison of various device parameters of GIGO TFTs as a function of process pressure

	Mobility (cm^2/Vs)	Vth (V)	S.S. (V/decade)	On/off ratio
1 mTorr	19.17	1.42	0.21	2.63×10^{10}
3 mTorr	16.13	2.95	0.27	1.63×10^{10}
5 mTorr	11.99	4.05	0.64	9.40×10^{8}

where W (1000 μm) is the channel width, L (150 μm) is the channel length, and Ci is the capacitance per unit area of the gate oxide. As the process pressure decreased from 5 to 1 mTorr, the μ_{SAT} and V_{th} values in GGIO TFTs were significantly improved from 11.99 cm^2/Vs and 4.05 V to 19.17 cm^2/Vs and 1.42 V, respectively. In addition, the S-value of 0.21 V/decade and Ion/off ratio of 2.63×10^{10} were also obviously improved for the device deposited under 1 mTorr. As reported in previous papers [8, 9], a significant improvement in device performance was observed for the TFTs utilizing a-IGZO channel deposited at a low pressure of 1 mTorr. They determined the reason for this improvement by physical analysis variation, wherein film density and roughness of the a-IGZO films deposited at different chamber pressures were evaluated. The composition change for the a-IGZO films was negligible, indicating that the compositional variation was not responsible for the observed pressure dependence of the device properties [8].

The density, roughness, and cation composition of the GGIO films deposited at different pressures were analyzed to confirm physical effect of pressure on the GGIO film quality. The compositions of GGIO films deposited at different process pressures were measured by Rutherford backscattering spectroscopy (RBS, not shown here), which also showed no significant changes for each element. Figure 2 shows the measured XRR data for the GGIO films as a function of process pressures, and summarized, as shown Table 2. The critical angle for total external reflection for the 1 mTorr sample was larger than that for the 5 mTorr sample, indicating that the GGIO film grown at 1 mTorr is denser than that at 5 mTorr. It was found that the density of the GGIO films increased from 6.43 to 7.38 g/cm3 with decreasing the chamber pressure from 5 to 1 mTorr. The surface root-mean-square roughness of GGIO films was also enhanced from 1.58 nm (5 mTorr) to 0.87 nm (1 mTorr), as shown in Table 2. These improvements could be attributed

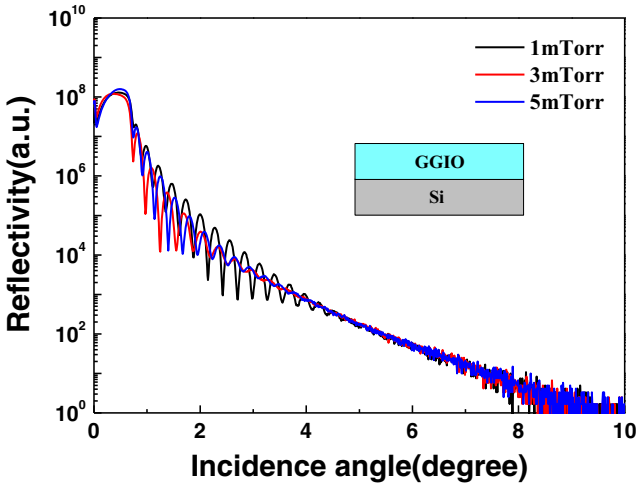

Fig. 2 X-ray reflectivity (XRR) curves on different process pressure

to increasing in the mobility of the ad-atoms on the film surface because the lower process pressure reduces the scattering of the sputtered species during deposition [8.9].

In order to look for other origins of device performance enhancement in terms of electronic structures as a function of process pressure, the band alignment of GGIO films deposited at different pressures was evaluated. Figure 3(a) shows the normalized O K1 edge spectra of the GGIO film. Normalizations of XAS spectra were carefully performed by subtracting the X-ray beam background and subsequently scaling pre- and post-edge levels, which can be used to compare the qualitative changes of the conduction band [20]. First, the O K1 edge spectra of GGIO films are directly related to the O p-projected states of the conduction band, which consists of unoccupied hybridized orbitals for In 5sp, Ge 4sp, Ga 4sp, and O 2p from 530 to 550 eV. The conduction band area is increased and the crystal field (C-F) splitting is enhanced upon reducing the process pressure. Thus, it is quite reasonable that the GGIO TFT may have the highest mobility value at 1 mTorr. To investigate the origin of the growing conduction band, the theoretical O K-edge XAS spectra of In_2O_3, Ge_2O_3, and Ga_2O_3, which were obtained from each material, were compared to the GGIO films, as shown in Fig. 3(b). Although the peak position of GGIO spectra might be different from those of binary oxides due to the different local coordination, the energy ranges of the unoccupied s/p orbitals for each element can be assessed approximately from the orbital energies of the binary oxides. Cho et al. [21] reported that the In 5 s band

Table 2 Roughness, density, and thickness of GGIO thin films as a function of deposition pressure

	Thickness (nm)	Density (g/cm^3)	Root-mean-square roughness (nm)
1mTorr	29.8	7.38	0.87
3mTorr	28.2	7.03	1.50
5mTorr	29.9	6.43	1.58

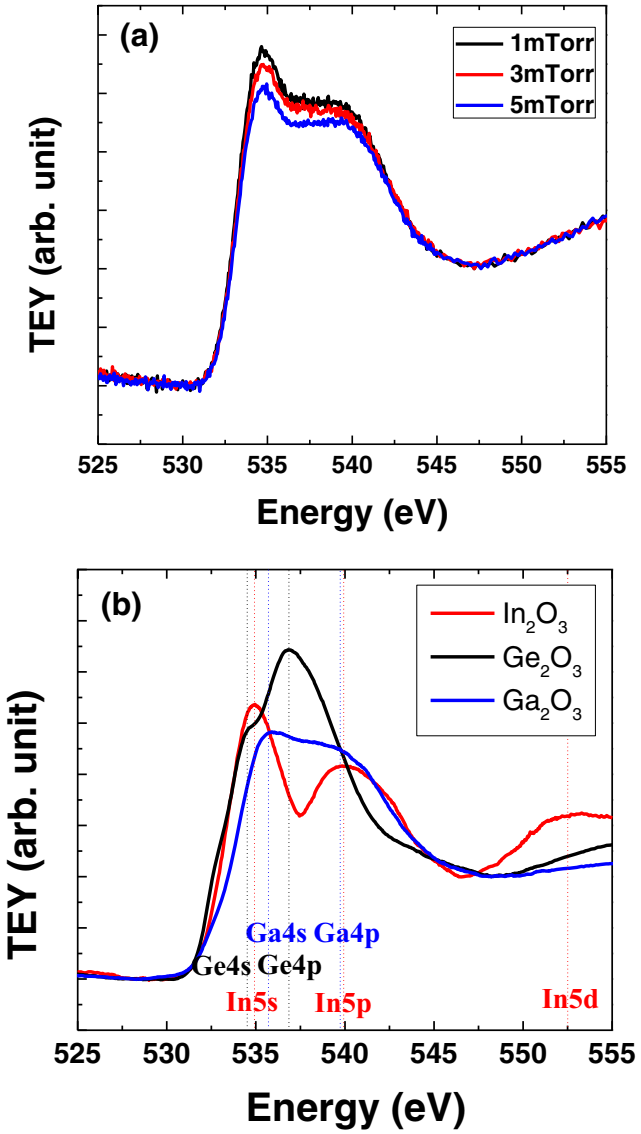

Fig. 3 (**a**) Normalized XAS O K_1 edge spectra of GGIO films as a function of deposition pressure. (**b**) The theoretical O K-edge XAS spectra of In_2O_3, Ge_2O_3, and Ga_2O_3

should be an electron source in the a-IGZO system by XAS analysis, in accordance with molecular dynamics calculation by Nomura et al. [10] The In 5 s band could also be an electron source in the GGIO system, as shown in Fig. 3(b).

The GGIO bandgap and the relative position of the Fermi level with respect to the valance band maximum were analyzed by SE and XPS, as shown in Fig. 4. The corresponding values of the bandgap (E_g) and relative energy difference between the Fermi level (E_F) and valence band maximum (ΔE_{VB}), and between E_F and conduction band minimum (ΔE_{CB}) are indicated below the diagram. The extracted bandgap increased from 3.61 to 3.68 eV with the increase of process pressure and the valence band offset (ΔE_{VB}) has a similar value regardless of process pressure. As a result, the relative position of the Fermi level (ΔE_{CB}) shifts far from the conduction band minimum, from 1.45 eV (1 mTorr) to 1.54 eV (5 mTorr), which is strongly correlated with the carrier concentration. Based on the above results, the most plausible origin of improved device operation and performance may be attributed to the enlargement of conduction band area caused by the change of In 5 s band. In addition, the increased carrier concentration in the GGIO channel layer observed by decreased process pressure resulted from the reduction of the conduction band offset.

Figure 5 shows the representative transfer curves and the shifts of threshold voltage on GGIO TFTs deposited at 1 mTorr as a function of the PBTS time. As the stress time passed, V_{th} systematically shifted in the positive direction without any significant changes of mobility and S.S values. Interestingly, after PBTS was applied for 10,800 s, the shift of V_{th} also decreased from 18.5 to 8.3 V with decreasing process pressure from 3 to 1 mTorr, as shown Fig. 4(b). Generally, the positive Vth shift in the PBTS condition was attributed to: electron trapping in the bulk deep trap and electron trapping in the interface trap (gate insulator and passivation layer) [13–15].

Thus, the trap density of GGIO deposited at different process pressures was measured using three methods, including: calculation by S.S value, MN rule, and SE analysis in order to determine the quantitative relationship of PBTS instability and trap density. Generally, the S.S value of a given TFT device is related to the total trap density, including the bulk GGIO channel layer (N_{SS}), and at GGIO/SiO_2 interfacial

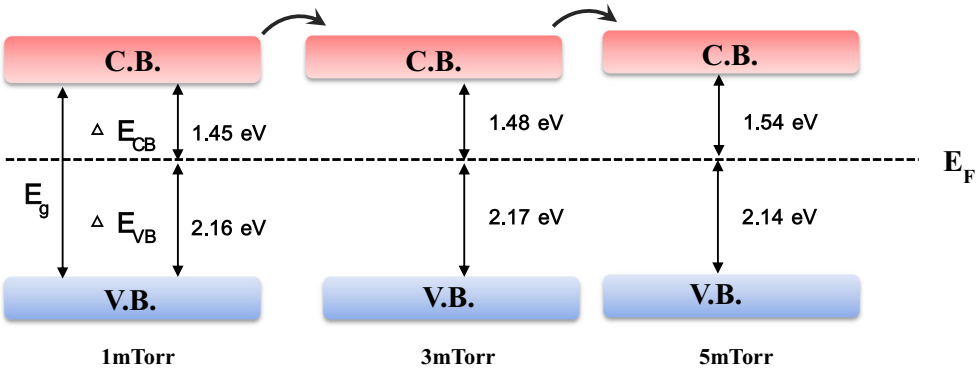

Fig. 4 Schematics of energy band diagrams of GGIO films at as a function of deposition pressure

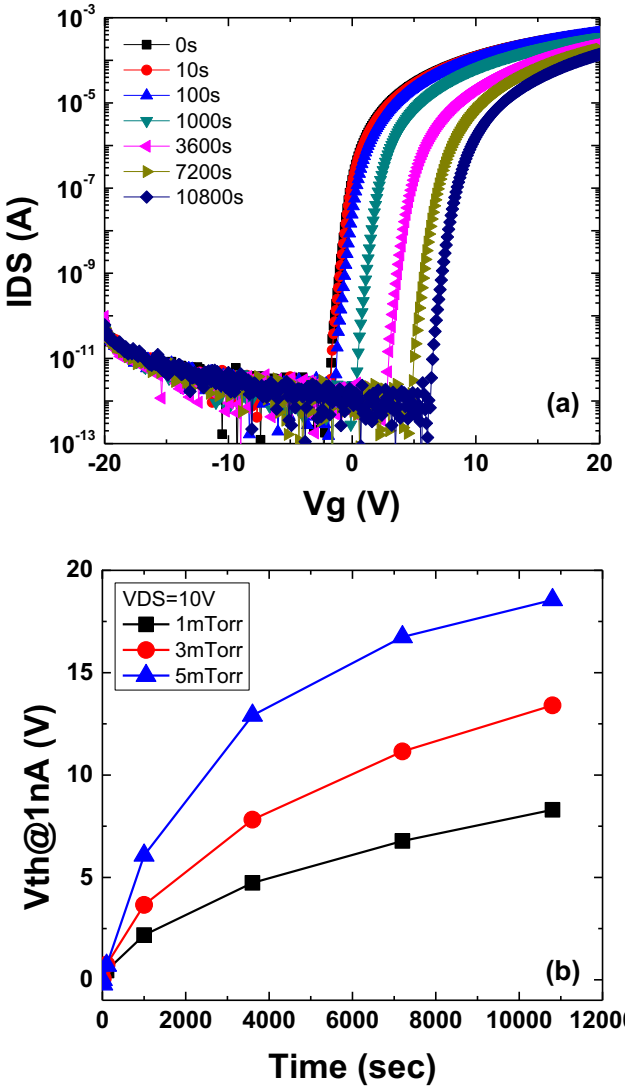

Fig. 5 (**a**) Representative evolution of transfer curves of GGIO TFT deposited at 1 mTorr and (**b**) the evolutionary shift of ΔV_{th} values on different process pressure (1, 3, 5 mTorr) as a function of stress time (stress condition: V_{GS}=20 V and 60 °C)

traps (D_{it}) as follows [19].

$$SS = \frac{qk_BT(N_{ss}t_{ch} + D_{it})}{C_i \log(e)} \quad (2)$$

where q is the electron charge, k_B is Boltzmann's constant, T is the absolute temperature, and t_{ch} is the channel layer thickness. We assumed that N_{SS} or D_{it} is separately set to zero in order to estimate the reduction in N_{SS} or D_{it} caused by changing the deposition pressure. It is noted that the values of N_{SS} and D_{it} calculated in this way correspond to the maximum densities [22]. The N_{SS} and D_{it} values for the device of deposited at 1 mTorr were 1.27×10^{17} /eVcm^3 and 6.34×10^{11} /eVcm^2, respectively. For the 5 mTorr deposited device,

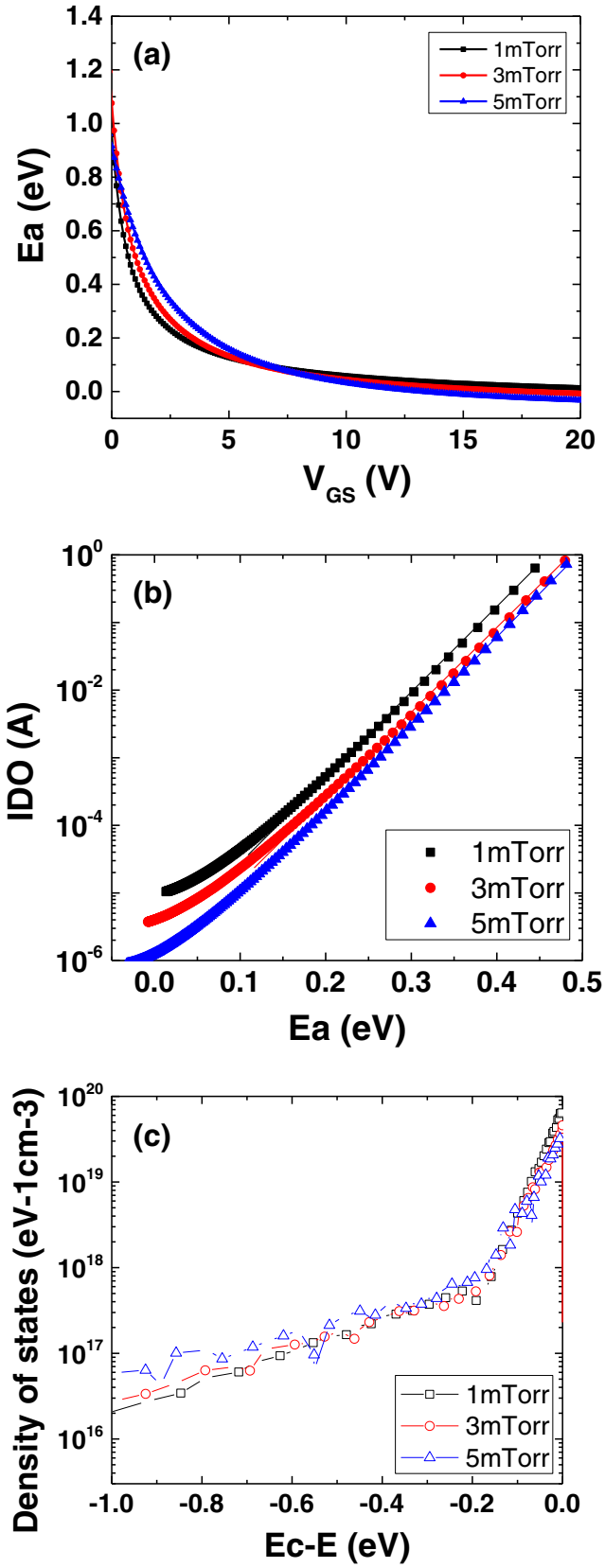

Fig. 6 (**a**) Activation energy (Ea) and (**b**) prefactor (I_{D0}) as a function of V_{GS} **c** calculated DOS distribution as a function of the energy (E-Ec) for GGIO TFTs deposited at different process pressures (1, 3, 5 mTorr)

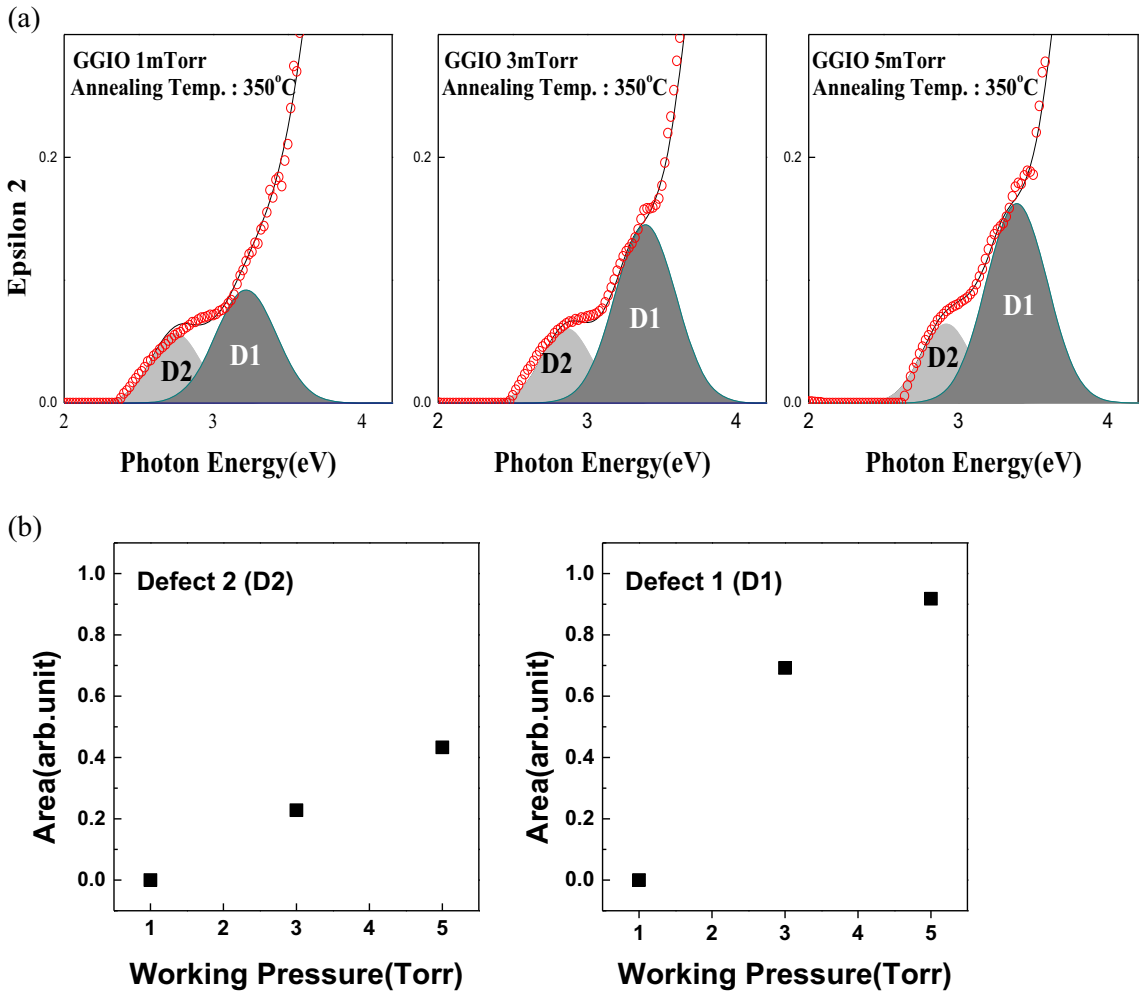

Fig. 7 (**a**) The band edge states over a narrow energy region below the conduction band edge. Two distinct deconvoluted peaks, labeled D1 and D2 are Gaussian fits (**b**) Relative area of band edge states (D1 and D2) as a function of process pressure

these values increased considerably to 3.87×10^{17} /eVcm^3 and 1.93×10^{12} /eVcm^2, respectively.

The temperature-dependent field effect data were used to calculate the near conduction band. We observed that the drain current (*ID*) is thermally activated and can be described by [23, 24]

$$I_D = I_{D0}\cdot\exp\left(-E_a/KT\right) \tag{3}$$

where I_{D0} is the prefactor, E_a is the activation energy, K is the Boltzmann constant, and T is the temperature. The E_a of GGIO TFT deposited at different process pressures are V_{GS}-dependent, and their relationship obeys the MN rule, as shown in Fig. 6(a). The E_a is the energy difference between the Fermi level and the edge of the conduction band, which equates to the average energy that a trapped electron needs to gain in order to escape from the localized state [23]. The activation energy value of the GGIO TFT decreased as deposition pressure was reduced. This implies that GGIO TFT deposited at a lower pressure has a much lower density of localized states near the conduction band than that at higher pressure. The MN rule is known to be an intrinsic property of a disordered semiconductor, and has been reported in various organic and inorganic semiconductor materials, including pentacene [25], a-Si [26], and a-IGZO [23]. Equation (4) is the MN rule formula [23],

$$I_{D0} = I_{D00}\cdot\exp(A\cdot Ea) \tag{4}$$

where A is the MN parameter, ID_{00} is a constant for a set class of materials. Using the MN relation, the subgap Density of stste (DOS) distribution can be extracted based on the assumption that most induced electron charges are occupied in the localized energy states, and the probability of finding an electron at a certain energy level is determined by 0 K Fermi statics, as reported Chen et al. [23]. The accurate flatband voltage (V_{FB}) and A values were determined by matching

the calculated activation energy with the measured activation energy, as shown in Fig. 6(b). Upon decreasing the deposition pressure from 5 to 1 mTorr, the calculated V_{FB} and A values were varied from −2.0 V and 30.8 eV^{-1} to −1.1 V and 29.5 eV^{-1}, respectively. In previous reports [23, 24], the calculated A value of the a-IGZO system by MN rule was in the range of 19–24.3 eV^{-1}, which varied by process condition and/or G/I material. The total DOS distribution for three devices deposited at different pressures was calculated, as shown in Fig. 6(c). Chen et al. reported that the DOS could be separated by two regimes, sub-threshold and above threshold, in a-IGZO TFT, since the two regimes exhibit different MN relations. In our results, the calculated GGIO DOS could be separated by sub-threshold (deep states, $<10^{18}$ $eVcm^{-3}$, E-Ec >0.2 eV) and above threshold (tail states and/or shallow level, $>10^{18}$ $eVcm^{-3}$, E-Ec <0.2 eV) regimes in GGIO TFT. The total DOS for a GGIO TFTs deposited at 1 mTorr was much smaller than that of a GGIO TFTs deposited at 5 mTorr over the 0.2–0.3 eV energy range (deep states) extracted. This result agreed qualitatively with the comparative results for the $N_{SS,\ max}$ values calculated from the SS value.

In order to investigate the DOS distribution of the GGIO films, SE data were analyzed as a function of process pressure in Fig. 7. Figure 7(a) shows the imaginary dielectric function (ε_2) spectra from SE measurements of a TIZO film deposited at different pressures with the deconvoluted Gaussian band edge states (D1, D2) using a simple four-phase model comprised of a Si substrate, SiO_2 overlayer, GGIO overlayer, and ambient layer. As the process pressure increased, the evolution of band edge states indicates that the shallow band edge state (D1, donor-like) is drastically increased and the deep band edge state (D2, accept-like) is slightly increased, as shown in Fig. 7(b). These results were consistent with the DOS distribution calculated by TFT measurement [27]. Therefore, extraction of the DOS for GGIO TFTs using the MN rule and that of the GGIO film itself by SE measurement will be quite useful for understanding the resulting PBTS instability.

4 Conclusions

The electrical properties, including device mobility and BTS-induced instability, of GGIO TFTs have been investigated at different deposition pressures. Under a lower process pressure of 1 mTorr, the mobility of 11.18 cm^2/Vs was increased and the ΔVth shift during PBTS for 3 h was also reduced by approximately 60 %. The GGIO film deposited at a lower process pressure showed a smaller conduction band offset ($\Delta E_{CB}=E_g - \Delta E_{VB}$) and increased conduction band area caused by change of the In 5 s band. In addition, the total amount of DOS located near the conduction band was reduced by decreasing the deposition pressure. These evolutions of electronic structure, such as the band alignment and band edge states of GGIO, are strongly correlated to the device characteristics of GGIO TFTs and are dependent on the process pressure.

Acknowledgments This work was supported by the RFID R&D program of MKE/KEIT. [10035225, Development of core technology for high performance AMOLED on plastic].

References

1. J.S. Park, H. Kim, I.D. Kim, J. Electroceram. **32**, 117 (2014)
2. J.S. Park, W.J. Maeng, H. Kim, J.S. Park, Thin Solid Film **520**, 1679 (2012)
3. J.S. Park, K. Kim, Y. Park, Y.G. Mo, H.D. Kim, J.K. Jeong, Adv. Mater. **21**, 329 (2009)
4. R.A. Street, Adv. Mater. **21**, 2007 (2009)
5. S.I. Kim, C.J. Kim, J.C. Park, I. Song, S.W. Kim, H. Yin, E. Lee, J.C. Lee, Y. Park, Electron. Devices Meet. IEEE Int. **2008**, 1 (2008)
6. J. Park, K.S. Son, T.S. Kim, J.S. Jung, K. Lee, W.J. Meang, H. Kim, E.S. Kim, K. Park, J. Son, J. Kwon, M.K. Ryu, S. Lee, IEEE Elect. Dev. Lett. **31**, 960 (2010)
7. Y.S. Rim, W. Jeong, B.D. Ahn, H.J. Kim, Appl. Phys. Lett. **102**, 143503 (2013)
8. J.H. Jeong, H.W. Yang, J.S. Park, J.K. Jeong, Y.G. Mo, H.D. Kim, J. Song, C.S. Hwang, Electrochem. Solid-State Lett. **11**, H157 (2008)
9. S. Yasuno, T. Kita, A. Hino, S. Morita, K. Hayashi, T. Kugimiya, J. Appl. Phys. **52**, 03BA01 (2013)
10. K. Nomura, T. Kamiya, H. Ohta, T. Uruga, M. Hirano, H. Hosono, Phys. Rev. B **75**, 035212 (2007)
11. T. Kamiya, K. Nomura, M. Hirano, H. Hosono, Phys. Status Solidi C **5**, 3098 (2008)
12. Y. Kim, M. Bae, W. Kim, D. Kong, H.K. Jeong, H. Kim, S. Choi, D.M. Kim, D.H. Kim, IEEE Trans. Electron. Devices **59**, 2689 (2012)
13. R.B.M. Cross, M.M. De Souza, Investigating the stability of zinc oxide thin film transistors. Appl. Phys. Lett. **89**, 263513 (2006)
14. J.M. Lee, I.T. Cho, J.H. Lee, H.I. Kwon, Appl. Phys. Lett. **93**, 093504 (2008)
15. A. Suresh, J.F. Muth, Appl. Phys. Lett. **92**, 033502 (2008)
16. S.Y. Lee, S.J. Kim, Y.W. Lee, W.G. Lee, K.S. Yoon, J.Y. Kwon, M.K. Han, IEEE Electron. Device Lett. **33**, 218 (2012)
17. S. Yang, D.H. Cho, M.K. Ryu, S.H.K. Park, C.S. Hwang, J. Jang, J.K. Jeong, Appl. Phys. Lett. **96**, 213511 (2010)
18. K. Nomura, T. Kamiya, H. Yanagi, E. Ikenaga, K. Yang, K. Kobayashi, M. Hirano, H. Hosono, Appl. Phys. Lett. **92**, 202117 (2008)
19. B.D. Ahn, H.S. Shin, H.J. Kim, J.S. Park, J.K. Jeong, Appl. Phys. Lett. **93**, 203506 (2008)
20. K.B. Chung, J.P. Long, H. Seo, G. Lucovsky, D. Nordlund, J. Appl. Phys. **106**, 074102 (2009)
21. D.Y. Cho, J.W. Song, K.D. Na, C.S. Hwang, J.H. Jeong, J.K. Jeong, Y.G. Mo, Appl. Phys. Lett. **94**, 112112 (2009)
22. M.K. Ryu, S.H. Yang, S.H.K. Park, C.S. Hwang, J.K. Jeong, Appl. Phys. Lett. **95**, 072104 (2009)
23. C. Chen, K. Abe, H. Kumomi, J. Kanicki, IEEE Trans. Electron. Devices **56**, 1177 (2009)
24. K.H. Ji, J.I. Kim, H.Y. Jung, S.Y. Park, Y.G. Mo, J.H. Jeong, J.Y. Kwon, M.K. Ryu, S.Y. Lee, R. Choi, J.K. Jeong, J. Electrochem. Solid State **157**, H983 (2010)
25. E.J. Meijer, N. Matters, P.T. Herwig, D.M. de Leeuw, T.M. Klapwijk, Appl. Phys. Lett. **76**, 3433 (2000)
26. R.E.I. Schropp, J. Snijder, J.F. Verwey, J. Appl. Phys. **60**, 643 (1986)
27. K.H. Lee, K.C. Ok, H. Kim, J.S. Park, Ceram. Int. **40**, 3215 (2014)